SIMULATION OF THE THERMOELECTRICALLY GENERATED MAGNETIC FIELD IN A SC NINE-CELL CAVITY

J. Köszegi†, O. Kugeler, J. Knobloch, Helmholtz-Zentrum Berlin, Germany

Abstract

Several studies [1-3] showed that thermocurrents generate a magnetic field in a horizontal cavity test assembly or cryomodule, which may get trapped during the superconducting phase transition. The trapped flux causes additional dissipation during operation and can therefore significantly degrade the cavity's quality factor. We simulated the distribution of the generated magnetic field for an asymmetric temperature distribution and compared the results to experimental findings. Furthermore, the impact of a growing superconducting area on the magnetic field distribution was investigated. The simulations complement the experimental studies because direct measurements are only feasible with a limited number of magnetic field probes and hence restricted to selected locations and orientations. The simulations allow to analyze the local data in the context of the whole system.

NUMERICAL SIMULATIONS

Setup

Figure 1 shows the model of a TESLA-style cavity which was used to simulate the magnetic field in the system. It includes the niobium cavity, the liquid helium vessel (titanium) and the magnetic shield. Several components of the setup were excluded (e.g. tuner, coupler) because they increased complexity as well as computation time without influencing the thermocurrent.

The bellow between cavity and tank was also omitted. However, its small wall thickness caused its DC resistance to be in the same order of magnitude as the helium tank itself. Hence, it had to be accounted to obtain a realistic thermocurrent value [4]. Thus, a thin ring was added to the vessel head. By use of this ring, the overall resistance of the system was tuned to simulate the experimental data from a vertical test which was presented in Reference [5]. The temperature dependent material properties needed for the calculations (heat capacity, thermal conductivity, electrical conductivity and thermopower) were taken from References [6-8].
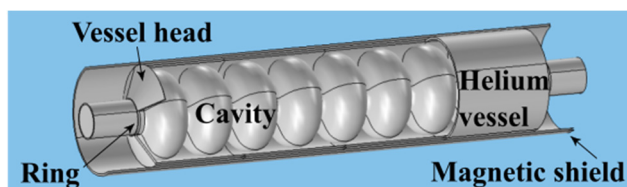

Figure 1: Model of cavity, magnetic shield and tank with ring for adjustment of electrical resistance.
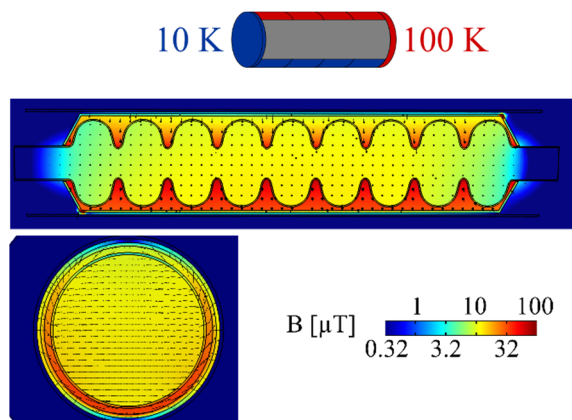
Figure 2: Magnetic field inside cavity and tank in a logarithmic scale for asymmetric temperature boundaries (displayed on top). The black arrows indicate the magnetic field vectors that point into and out of the paper plane in the middle figure and from left to right in the bottom figure.

Steady State Boundary Conditions

The thermocurrent in the cavity-tank-system is driven by large temperature differences which occur during the cool down procedure. In the cool down scheme commonly used in horizontal operation, the liquid helium is filled via a filling line at the bottom left of the tank.

Based on the experimental conditions, two temperature gradients were implemented in the simulations: first a gradient from left to right driving the thermocurrent. Second, a gradient from bottom to top which must be included because it breaks the symmetry of the current distribution. Without the second gradient, no magnetic field would be present at the RF surface inside the cavity [2, 3].

Results

Figure 2 shows the magnetic field obtained for asymmetric temperature distribution over the whole length of the cavity. The vessel heads were set to 10 K and 100 K for the first gradient and, in addition, the bottom quarter of the helium tank was set to 10 K and the top quarter to 100K for the second gradient as is depicted in the uppermost image.

The resulting distribution is in general comparable to simulations presented previously [2, 3]. In addition, we found that the magnetic field inside the cavity is more homogeneous due to the magnetic shield which is placed closely around the helium vessel.

Furthermore, the field inside the cavity is oriented orthogonally to the bottom to top gradient. Since the vessel
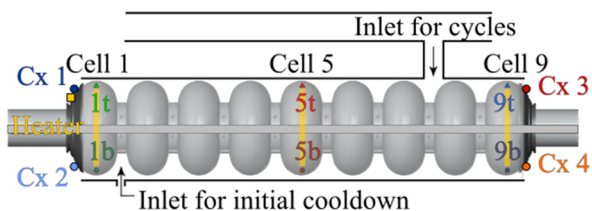
Figure 3: Positions of four Cernox (Cx) sensors outside and six fluxgate magnetometers (labelled with cell number 1/5/9 and location t/b) inside the cavity.

heads are set to a constant temperature, the asymmetry and hence magnetic field in cells 1 and 9 are reduced.

In the cells 2 to 8, it ranges from 8 µT to 14 µT. The maximum in each cell is at the bottom and the field decreases towards the top. The result has the correct order of magnitude to explain the increased residual resistance in the RF tests [1-3].

DIRECT MEASUREMENT

Setup

The calculated magnetic field between the tank and the cavity (Figure 2) agrees with previous experimental data [5]. However, the field *inside* the cavity at the RF surface is not only determined by the amplitude of the thermocurrent but mainly by the asymmetry. Hence, the simulated values inside the cavity have to be verified by a measurement as well.

For that purpose, a TESLA-style cavity similar to those in previous experiments was equipped with six fluxgate magnetometers from the inside. The setup of the sensors is shown in Figure 3. The sensors were placed in the bottom and in the top of the equator in cells 1, 5 and 9.

Results

The setup was used to track the change in magnetic field during warm up and cool down of nine thermal cycles. Detailed data on the study can be found in Reference [9]. In this work, we focus on the level of trapped magnetic flux in the sc state after the cavity was in thermal equilibrium.

Figure 4 displays the measured level of trapped magnetic flux as a function of average temperature difference ΔT during the respective phase transition. ΔT was calculated when the first Cx sensor dropped below the transition temperature as $\Delta T = | (T_{Cx1}+T_{Cx2})/2 - (T_{Cx3}+T_{Cx4})/2 |$. The figure shows that the simulation of complete asymmetry given in Figure 2 provides a reasonable approximation for the highest values of trapped flux which were obtained in cell 9 – the cell which transition first (8.3 µT for ΔT = 71 K). The other cells showed lower values of trapped flux.

The decrease can be explained by the time lag between the transitions from cell to cell. By the time when cells 5 and 1 transitioned, the temperature difference between the cavity-tank-joints had already reduced. The time lag between transitions in cells 1 and 9 was approximately 5 to 10 min for the various thermal cycles which was enough time for the temperature difference to drop by several 10 K.
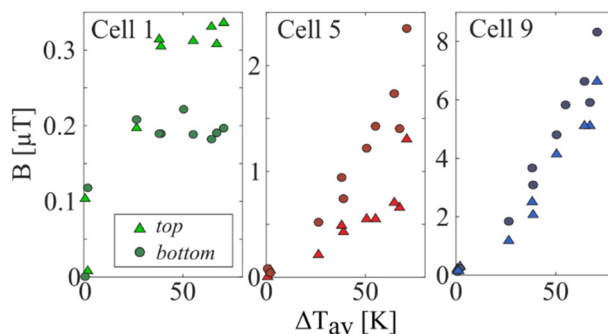

Figure 4: Direct measurement of the trapped flux inside the cavity by six fluxgates.
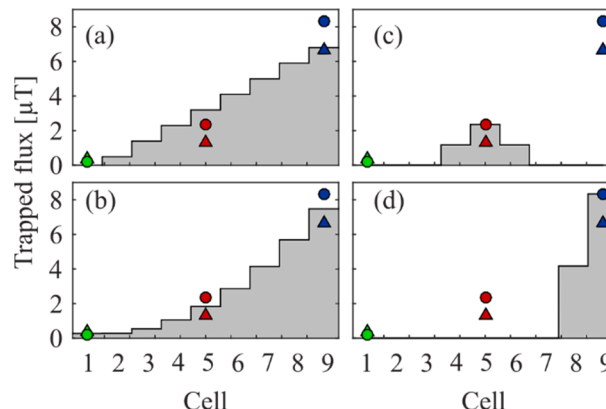

Figure 5: Directly measured trapped flux in cells 1, 5 and 9 together with conceivable distributions of trapped magnetic flux (grey) in all nine cells for one example cycle.

Finally, cell 1 transitioned into the sc state. It exhibited only a maximum of 0.35 µT trapped flux and no significant increase due to thermocurrents for any thermal cycle because the temperature difference had already vanished to the most part by the time cell 1 transitioned.

In addition to the decrease along the cavity, we found that the niobium in the bottom trapped more flux compared to the top in cells 5 and 9 which might also be caused by a time lag since all cells transitioned bottom first.

Based on the direct measurement of the trapped magnetic flux in three cells and on the simulations, we constructed conceivable distributions of trapped flux for all nine cells. Figure 5 shows a linear (a) and a quadratic (b) distribution along the cells. Furthermore, we added models of trapped flux including only the middle (c) or end (d) cells for comparison.

Comparison to RF Data

Reference [2] presented measurements of the surface resistance in three passband modes. It included an analysis of the residual resistance R_{res} in the 8/9 π and 1/9 π modes as a function of the π mode R_{res}. The data allowed a first estimate of the surface resistance distribution over the whole cavity. The data was later combined with the directly measured data shown in Figure 4.
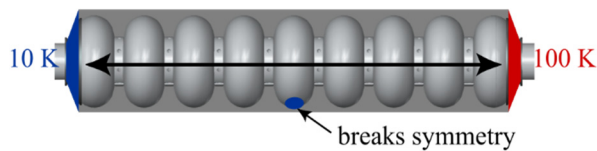
Figure 6: Setup for the calculation of the magnetic field distribution caused by a thermocurrent considering a growing sc spot.

Based on the combination of the two data sets, we were able to show that trapped flux distributions which consider only selected cells (c, d) do not fit with the RF data at all [9].

However, the continuous interpolations (a, b) gave reasonable results where the linear distribution fitted better for the $1/9\,\pi$ mode while the quadratic distribution fitted better for the $8/9\,\pi$ mode. The result hints that the actual distribution of thermoelectrically generated trapped magnetic flux along the TESA cavity is somewhere in between linear and quadratic.

To this point we investigated the level of trapped magnetic flux in the sc state after the cavity reached thermal equilibrium. The data was compared to a simulation which assumed an asymmetry in the temperature distribution over the whole length of the cavity *before* the phase transition (Figure 2). The calculation yielded results consistent with the maximum level of trapped magnetic flux observed in the measurement. However, the actual asymmetry in the system is largest once the first sc area establishes.

Hence, we continue with a second set of simulations investigating the asymmetry caused by the appearance of the first sc spot which subsequently grows. The results of the calculations are then compared to previous experiments presented in Reference [10].

THE SUPERCONDUCTING PHASE TRANSITION

Simulation Setup

In the simulations, the superconducting material is implemented as niobium with modified material properties. The electrical conductivity is increased by a factor of 10^3 and μ_r is set to 10^6 to simulate (almost) vanishing DC resistance and almost perfect diamagnetism. The thermal properties are not changed.

The goal of the simulations is to investigate the influence of the localized appearance of superconductivity independently of other sources of asymmetry. Hence, the setup is designed based on a symmetric temperature distribution, which provides the same driving force for the thermocurrent as in the previous simulations but without embedded asymmetry.

A round area at the bottom of the equator of cell 5 is defined and set to the modified niobium properties to simulate the superconducting spot without manipulating the temperature distribution. Thereby, the superconducting area is not below the transition temperature, which does not matter because the properties are artificially set superconducting.

The setup is depicted in Figure 6. It allows an estimate of the field distribution after the onset of phase transition without the necessity of implementing a complicated temperature distribution.
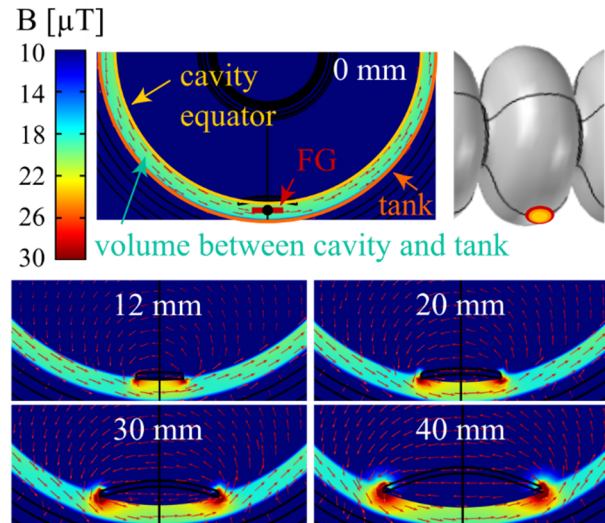

Figure 7: Magnetic field distribution around a growing sc spot. Black dot on top of FG in first graph: ``FG position'' used for evaluation. White numbers give the diameter of the sc spot in the respective simulation.

Results

Figure 7 shows the results of the simulations. The numbers give the diameter of the spot and the black dot in the first plot gives the "FG position" at which the magnetic field values are compared.

In the symmetric case prior to the sc transition (0 mm spot diameter), the field value is 20 µT. For the smallest sc spot simulated (12 mm), the field increases to 22.6 µT. At the edge of the superconducting area, the field even reaches a value of 31 µT.

With increasing spot size, the magnetic field at the FG position decreases towards the value of the symmetric case. The field at the edge, however, increases due to the implemented Meissner effect.

The data presented in Figure 7 can be compared to previous direct measurements of magnetic field from Reference [10]. In the measurements, the temperature was measured in the same way as shown in Figure 3. The FGs, however, were positioned inside the tank and not inside the cavity.

The benefit of measuring inside the tank is that the instrumentation does not interfere with any RF tests performed on the cavity. The drawback is that the measurement mainly gives information on the thermoelectrically generated magnetic field in the complete system but not specifically at the RF surface.

Comparison to Experimental Data

The calculated values in Figure 7 can be compared to the previous experimental results. In Reference [10] it had been demonstrated that the thermoelectrically generated magnetic field in the tank exhibits a peak during the sc

phase transition even though the temperature difference driving the current was already decreasing.

The peak was typical and very reproducible for any thermal cycle with a significant temperature difference along the cavity-tank system. Furthermore, its amplitude was directly correlated to the RF dissipation as well. We therefore conclude that the peak value measured in the tank indicates the amount of thermocurrent in the complete system which directly translates into trapped flux.

The origin of the peak can now be understood based on the presented simulations. The comparison with experimental data shows how the magnetic field present in the symmetric case gets enhanced once a sc spot establishes. It is maximal at the edge of the sc area where the phase front is located. The maximum value, computed for the smallest area size of d = 12 mm is 31 µT. The value corresponds to a field enhancement one third compared with the symmetric case. In the experimental data, the field enhancement was repeatedly also one third.

Based on the presented results we can furthermore understand the correlation of RF dissipation and magnetic field peak value shown in Reference [10]. The change in peak height between different cycles, if measured at the same position and for similar temperature distributions, corresponds to the change in overall amount of thermocurrent in the system. The more thermocurrent is flowing, the higher is the resulting peak in magnetic field during transition and vice versa. Finally, the thermoelectrically generated magnetic flux is trapped during the phase transition and increases dissipation during operation.

CONCLUSION

We presented a study combining numerical simulations and experimental data to assess the distribution, amplitude and orientation of trapped flux caused by thermoelectrically generated magnetic field in a multi-cell cavity.

The analysis allowed a detailed understanding of the effect especially during the sc phase transition. Based on the present results, only limited diagnostics in the LHe tank of any cavity is needed to correctly assess the overall thermocurrent in the system.

ACKNOWLEDGMENTS

REFERENCES

[1] J. Vogt, O. Kugeler, and J. Knobloch, "Impact of cool-down conditions at Tc on the superconducting RF cavity quality factor," *Phys. Rev. ST Accel. Beams*, vol. 16, p. 102002, Oct. 2013.

[2] J. Vogt, O. Kugeler, and J. Knobloch, "High-Q operation of superconducting RF cavities: Potential impact of thermocurrents on the RF surface resistance," *Phys. Rev. ST Accel. Beams*, vol. 18, p. 042001, Apr. 2015.

[3] R. Eichhorn *et. al.,* "Thermocurrents and their role in high Q cavity performance," *Phys. Rev. Accel. Beams*, vol. 19, p. 012001, Jan. 2016.

[4] A. Crawford, "A study of thermocurrent induced magnetic fields in ILC cavities", arXiv:1403.7996v1, 2013.

[5] J. Vogt *et. al.,* "Fermilab studies of quality factor changes of a N doped cavity from vertical to dressed horizontal test", TTC meeting, KEK, 2014.

[6] J. Köszegi, "Surface resistance minimization in SRF cavities by the reduction of thermocurrents and trapped flux", PhD. thesis. Universität Siegen, 2017.

[7] J. Jensen, R. Stewart, W. Tuttle, H. Brechna, and A. Prodell, "Selected cryogenic data notebook, vol. 2," Brookhaven National Laboratory, 1980.

[8] M. Merio and T. Peterson, "Material properties for engineering analysis of SRF cavities," Fermilab Specification: 5500.000-ES-371110, 2011

[9] J. Köszegi *et. al.,* "Simulation of the thermoelectrically generated magnetic field in a sc nine-cell cavity", in *Proc. IPAC'17*, Copenhagen, Denmark, May 2017, paper MOPVA048, pp.968-970.

[10] O. Kugeler *et. al.,* "Horizontal testing and thermal cycling of an N-doped TESLA-type cavity", in *Proc. SRF'15*, Whistler, Canada, September 2015, paper MOPB019, pp.126-128.